doi:10.14311/ppt.2025.1.40
Plasma Physics and Technology **12**(1):40–45, 2025

MODELLING STUDIES OF ARCS OF SHORT LENGTH BETWEEN COPPER ELECTRODES

M. Baeva[a,*], J. K. C. Ballentin[b], D. Uhrlandt[a,b]

[a] *Leibniz Institute for Plasma Science and Technology, Fellix-Hausdorff-Str. 2, 17489 Greifswald, Germany*
[b] *Institute for Electrical Power Engineering, University of Rostock, 18051 Rostock, Germany*
[*] baeva@inp-greifswald.de

Abstract. In this work, we focus on the electrical properties of arcs of length of a few millimeters at a current level of 2 A. The computation is based on a unified non-equilibrium model that resolves the entire inter-electrode region, applies a deformed mesh to simulate the contact opening, and couples the heat transfer to the electrodes. The arcs are burning in atmospheric pressure air at the presence of Cu metal vapour. Experimental findings are used to calibrate the model.

Keywords: modelling, DC short arcs, air-copper, atmospheric pressure.

1. Introduction

Low-voltage, low-current arcs of short lengths that occur in air in presence of copper metal vapour are related to electrical switching applications. These arcs occur mostly in the breaking operation, i.e., when the copper contacts under current are separated. The general understanding is that during the initial stage of separation, the electric current is enforced to flow through tiny protrusions while the most of the contact surface is already separated. This leads to increase of the current density and the Joule heating, which results in melting and evaporation of the remaining bridges [1, 2]. The copper metal vapour fills the discharge gap. With the further increase of the discharge gap the surrounding air mixes with the metal vapour.

The characterization of these discharges is of current interest due to the increased demand in automotive applications and other low- direct current (DC) networks as well as for the reason of fundamental understanding. The experimental determination of the arc properties is reported in quite limited number of studies [3]. Modelling works can complement experimental studies and contribute to the characterization of the arcs as the spatial resolution of these small-size objects was enabled in recent years.

In a previous work [4], we applied a unified one-dimensional (1D) model to describe the arc plasma in air between cold copper (Cu) electrodes. The results indicated the occurrence of multiple reversals of the electric field and the anode voltage drop. Another work [5] reported on the modelling of an atmospheric pressure microdischarge in metal vapour of copper during the initial phase of contact opening. A small amount of air was considered as a background gas for gap lengths of 30 µm and 300 µm. The results showed a significant decrease of the arc voltage in comparison to pure air and the influence of the field enhancement factor (FEF) and the discharge radius (R_{dis}) on the discharge properties.

The present work considers modelling studies of the arc behaviour in atmospheric pressure air in presence of copper metal vapour. The model's settings are assumed to represent the stage of contact opening when the surrounding air has replaced in a large amount the metal vapour. The modelling studies are supported by experimental findings that provide the temporal behaviour of the arc voltage during the increase of the gap length up to 3 mm at a DC current of 2 A. Such studies have not be reported so far. The results of the modelling work are therefore its most salient and novel aspects.

2. Computational method

An almost complete description of the unified non-equilibrium model was given in [5] and therefore, a brief overview of the main features is given in what follows. The model solves the fluid equations for conservation of particles and energy of electrons and heavy particles, and the heat transfer in the electrodes. These equations are written as follows

$$\frac{\partial n_\mathrm{e}}{\partial t} + \nabla \cdot \mathbf{\Gamma}_\mathrm{e} = S_\mathrm{e}, \tag{1}$$

$$\frac{\partial n_\varepsilon}{\partial t} + \nabla \cdot \mathbf{\Gamma}_\varepsilon + e\mathbf{E} \cdot \mathbf{\Gamma}_\mathrm{e} = S_\varepsilon - Q_\mathrm{h} - Q_\mathrm{rad}, \tag{2}$$

$$\rho \frac{\partial Y_k}{\partial t} + \nabla \cdot \mathbf{J}_k = S_k, \tag{3}$$

$$\rho C_\mathrm{p} \frac{\partial T}{\partial t} + \nabla \cdot \mathbf{q} = Q_\mathrm{h} + Q_\mathrm{ionJ}. \tag{4}$$

The heat transfer in the electrodes is written as

$$\rho_\mathrm{s} C_\mathrm{ps} \frac{\partial T}{\partial t} + \nabla \cdot \mathbf{q}_\mathrm{s} = 0. \tag{5}$$

In equations (1)–(4), n_e and n_ε denote respectively the electron number density and the density of electron energy, e is the elementary charge, $\mathbf{\Gamma}_\mathrm{e}$ is the

electron particle flux, and $\mathbf{\Gamma}_\varepsilon$ is the electron energy flux. S_e and S_ε are source terms accounting respectively for the gain or loss of electrons and electron energy in inelastic processes. The terms Q_h and Q_rad describe respectively the loss of electron energy due to elastic collisions with heavy particles and volumetric radiation. ρ is the total mass density, Y_k, $\mathbf{J}_k$, and S_k denote respectively, the mass fraction, the mass flux, and the volumetric gain or loss of species of kind k.

The classical drift-diffusion approximation is applied to the electrons, so that the electron particle flux $\mathbf{\Gamma}_\mathrm{e}$ and the electron energy flux $\mathbf{\Gamma}_\varepsilon$ in equations (1) and (2) are expressed as containing components due to drift in the electric field $\mathbf{E}$ and due to gradients of n_e and n_ε.

In Eqs. (4) and (5), C_p denotes the specific heat capacity at constant pressure, $\mathbf{q}$ is the heat flux due to heat conduction. The subscript s denotes the quantities corresponding to the solids. Further, the term Q_ionJ in Eq. (4) represents the Joule heating of the ions.

The multi-component diffusion of species is solved in terms of a mixture-averaged model accounting for a full expression of diffusivity and a mixture diffusion correction. The plasma-chemical model is based on the 11 species reaction scheme for air [6] with atoms and singly charged ions of copper being added up. A special treatment is applied to obtain the rate coefficients for electron impact ionization and 3-body recombination of the Cu species taking into account the large number of excited states of Cu atoms. It is based on the modified diffusion approach [7], in which the ionization and recombination represent diffusion of bound electrons over the energy levels.

A Maxwellian distribution of the electron velocity is assumed with the electron temperature T_e, while the heavy species (atoms, molecules, ions) are considered in equilibrium at a common temperature T.

The electric potential, V, is obtained by solving the Poisson's equation

$$\Delta \mathrm{V} = -\frac{\rho_\mathrm{q}}{\varepsilon_0}, \tag{6}$$

where ρ_q is the space charge density, and ε_0 is the vacuum permittivity. The self-consistent electric field, E, follows from $\mathbf{E} = -\nabla V$.

The electric current density in the discharge $\mathbf{j}$ is composed of the particle flux of electrons ($\mathbf{\Gamma}_\mathrm{e}$) and the total of particle fluxes of ions of kind i ($\mathbf{\Gamma}_i$), i.e. $\mathbf{j} = -e(\mathbf{\Gamma}_\mathrm{e} - \Sigma_i \mathbf{\Gamma}_i)$. Its value is controlled by the electric current in an external electric circuit including a voltage source U_0 and a ballast resistance R_b, and the surface area of the electrodes S. Therefore, an equation for the external circuit is added to equations (1)–(6)

$$V_\mathrm{a} = U_0 - I R_\mathrm{b}, \tag{7}$$

where $I = \int_S \mathbf{n} \cdot \mathbf{j} dS$ denotes the electric current collected on S, and V_a is the potential at the anode.

Boundary conditions to equations equations (1) and (2) on the electrodes are written in terms of fluxes as follows

$$\mathbf{n} \cdot \mathbf{\Gamma}_\mathrm{e} = \frac{1}{4} n_\mathrm{e} v_\mathrm{th,e} - \gamma \Sigma_i \mathbf{\Gamma}_i \cdot \mathbf{n} - \mathbf{\Gamma}_\mathrm{tf} \cdot \mathbf{n}, \tag{8}$$

$$\mathbf{n} \cdot \mathbf{\Gamma}_\varepsilon = \frac{1}{4} n_\mathrm{e} v_\mathrm{th,e} \cdot 2 k_\mathrm{B} T_\mathrm{e} - \gamma \Sigma_i \epsilon_{\mathrm{se},i} \mathbf{\Gamma}_i \cdot \mathbf{n} - \epsilon_\mathrm{tf} \mathbf{\Gamma}_\mathrm{tf} \cdot \mathbf{n}. \tag{9}$$

The terms included in equations (8) and (9) represent in the order of their appearance contributions due to thermal diffusion of electrons to the electrode, secondary and thermo-field emission of electrons. The current density due to thermo-field electron emission from the Cu cathode, $j_{TF}(E, T_w)$, and the effective work function, $W'(E, T_w)$, are obtained using the Transferred Matrix Method [8] with T_w being the wall temperature of the cathode.

The boundary conditions to the equation for transport of heavy species of kind k (equation (3)) read

$$\mathbf{n} \cdot \mathbf{\Gamma}_k = \frac{1}{4} n_k v_{\mathrm{th},k} + a \mu_i n_k \mathbf{E} \cdot \mathbf{n}. \tag{10}$$

The thermal balance of the electrodes implies heat conduction and plasma-wall interaction that can result in melting and evaporation of the electrode material. The boundary conditions to equations (4) and (5) employ a fixed temperature for the anode and the cathode ends, which are not in contact with the plasma. On the edge between the plasma and the electrodes, heat fluxes Q_c and Q_a are introduced to account for contributions from the plasma to the heating/cooling of respectively the cathode and the anode. These fluxes add up the heat fluxes due to thermal conduction and are expressed as

$$\begin{aligned} Q_\mathrm{c} = \sum_i \left(j_{\mathrm{ion},i}(E_{\mathrm{ion},i} - W) - j_{\mathrm{se},i}(E_{\mathrm{ion},i} - W)\right) \\ - j_\mathrm{tf} W' + \frac{1}{4} n_\mathrm{e} v_\mathrm{th,e} (2 k_\mathrm{B} T_\mathrm{e} + eW) - \epsilon_\mathrm{c} \sigma_\mathrm{SB} T_\mathrm{w}^4 \\ - \pounds_c J_{vap,c} m_{v,c}, \end{aligned} \tag{11}$$

$$\begin{aligned} Q_\mathrm{a} = \sum_i \left(j_{\mathrm{ion},i}(E_{\mathrm{ion},i} - W_a)\right) \\ + \frac{1}{4} n_\mathrm{e} v_\mathrm{th,e} (2 k_\mathrm{B} T_\mathrm{e} + eW_a) - \epsilon_\mathrm{a} \sigma_\mathrm{SB} T_\mathrm{w,a}^4 \\ - \pounds_a J_{vap,a} m_{v,a}, \end{aligned} \tag{12}$$

The thermodynamic properties of the species are implemented as functions of the gas temperature in the region from 300 K up to 20000 K [9]. Data for the radiation losses [10] are considered in the energy balance of the electrons since the the excitation of copper atoms is considered to originate from collisions with electrons. The energy losses due to radiation are then related to the thermal balance of the gas as

well because electrons and heavy particles exchange energy in elastic collisions.

The model is realized as one-dimensional on the computational platform COMSOL Multiphysics®. The differential equations are solved applying a time-dependent direct solver PARDISO and a fully coupled non-linear approach based on the Newton method. This allows us to solve all dependent variables within a single iteration. The initial time step is 1×10^{-13} s. An automated increase is enabled in case the convergence criteria are satisfied.

The radial extent of the discharge is needed for realistic values of the electric current density. Estimates are obtained from high-speed imaging in the experiments [11]. The radial extent of the discharge (R_{dis}) is defined as a function of the time of motion and is modified during the contact separation. It can be scaled by introducing a scaling factor F_{Rdis}. The contact separation is simulated by the deformed mesh method. The computational grid in the discharge gap typically has 5000–6000 mesh elements as their size is exponentially decreasing toward the electrodes. The discretization of the electrodes applies 200 mesh elements as their size is linearly increased toward the ends. The simulations are performed like the experiments, i.e. the discharge is burning for 11 ms in a gap with a length of 30 µm before the contacts are separated within 52 ms with a constant speed so that the gap length is increased up to 3 mm.

3. Electrical measurements

A description of the experimental methods applied to the studies of electric arcs that are of relevance to the present work is provided in [11]. For the sake of completeness, a summary of the electrical measurements is given here.

To ignite the microarc, a 2 A DC pulse is sent through two opening copper electrodes. The experiment is conducted in ambient air at atmospheric pressure. During the opening process, the microarc voltage is measured using a digital oscilloscope (Yokogawa DLM2054). A step motor is used to set one electrode in a reproducible motion, while the position of the second electrode is fixed. The electrical diagnostics are complemented by optical data providing the radius of the discharge at different instances and positions, a high-speed camera (Photron Fast-Cam NOVA R3) records the arc formation in parallel with a frame rate of up to 10000 s^{-1} and exposure times down to 2 µs.

4. Results and discussion

Experimental finding obtained by means of electrical measurements, high-speed imaging, and optical emission spectroscopy [11] provide the arc voltage, images of the discharge and indication of presence of copper metal vapour during the contact opening. Although experimental results can scatter due to discharge instabilities and a reliable evaluation of the copper content is not currently available, the data are important to the settings of the model. Based on experimental data it is assumed that the radial extent of the discharge increases with the increase of the gap length. This means that a cylindrical shape of the discharge is assumed preserved in the framework of the 1D model. In reality, the discharge radius appears larger in the middle part of the gap.

Another important issue in the model is the treatment of the electron emission from the non-refractory copper cathode [8]. The electron emission current density is pre-computed as a function of the electric field (E) at the cathode surface and the temperature (T_w) on the cathode surface. The formation of cathode spots cannot be captured by the 1D model but it can be assumed that the model considers values of E and T_w corresponding to those of a spot. A FEF, which multiplies the electric field obtained from the Poisson's equation ($E \cdot FEF$) is introduced to account for a surface roughness and/or a presence of protrusions that cannot be otherwise captured in the 1D model. The FEF is another model parameter that can be adjusted in comparisons with the measured voltage. Note that the evaluation of the electron emission current density can include effects of lowering of the surface potential barrier for the electrons due to the Schottky effect but also a splitting of the barrier caused by presence of ions near the cathode surface. The latter leads to ion-enhancement of the electron emission and depends on the position of the ion. An account of this effect is not included yet but will be studied in forthcoming works.

Furthermore, a variation of the copper content in the gas mixture has been carried out in order to show its effect on the plasma parameters and find values in particular of the arc voltage, which agree with the measured one. Note that the lowering of the copper content in the plasma is limited by the accuracy of the multi-diffusion problem. The accuracy of the solutions becomes critical for a mole fraction of the copper vapour below $\sim 1 \times 10^{-3}$.

Simulations are performed starting with a discharge burning with a minimum gap length of 30 µm for a physical time of 11 ms. The contacts are further separated until the gap length reaches a value of 3 mm with a time of moving 51 ms. The increase of the gap length proceeds with a movement of the anode. These conditions correspond to the series of experiments carried out for a DC current of 2 A. In the simulations, the discharge radius, the field enhancement factor, and the mole fraction of Cu-vapour are varied in order to match the model and the experiment. The results obtained are presented in what follows.

Figure 1a shows the adopted discharge radii as a function of the distance from the cathode. A curve with a scaling factor of unity is considered as basic along with scaling factors of 1.1, 1.2, and 1.3. Simulations are performed for the various scaling factors (F_{Rdis}) of the discharge radius. The field enhancement

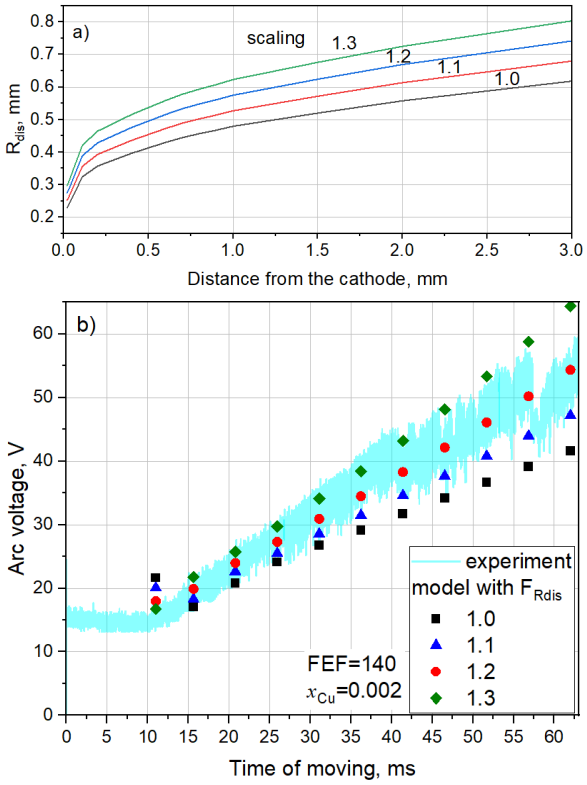

Figure 1. a) Variation of the discharge radius, b) Measured and computed arc voltage. The simulations are performed with FEF=140 and x_{Cu}=0.002.

factor is considered with a value of FEF=140 and the mole fraction of Cu-vapour is x_{Cu}=0.002. The predicted arc voltage is presented in comparison with experimental values, which are measured during the moving of the anode. The results show that predicted voltage increases with the increase of the discharge radius, which means a decrease of the current density at a constant current. The best match is obtained with a scaling factor of 1.2. This value is kept for the further simulations.

Figure 2 shows results obtained with a variation of FEF, while the mole fraction of Cu-vapour is x_{Cu}=0.002 and the scaling factor of the discharge radius is F_{Rdis}=1.2. The FEF implicitly increases the electric field on the cathode surface and the thermo-field electron current density. The higher factor leads to lower values of the arc voltage. The best match of predicted and measured values is achieved with FEF=140. Note that FEF controls the electron emission the cathode. The current density on the cathode contains components due to thermo-field emission, secondary electron emission caused by ion bombardment (plays a negligible role), back diffusion of electrons from the plasma, and ion drift to the cathode. The FEF value can change the ratio of the electron and ion current components on the cathode with respect to the total current density.

Figure 3 shows the computed and measured values of the arc voltage for various mole fractions x_{Cu} of the Cu-vapour in the mixture for F_{Rdis}=1.2 and

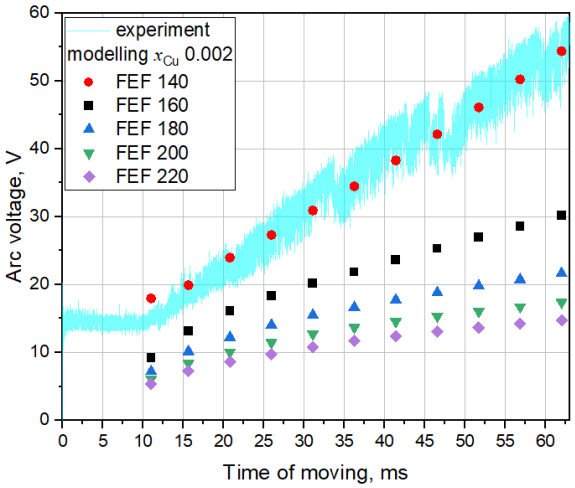

Figure 2. Computed and measured arc voltage for various FEF values. The simulations are performed with x_{Cu}=0.002 and F_{Rdis}=1.2.

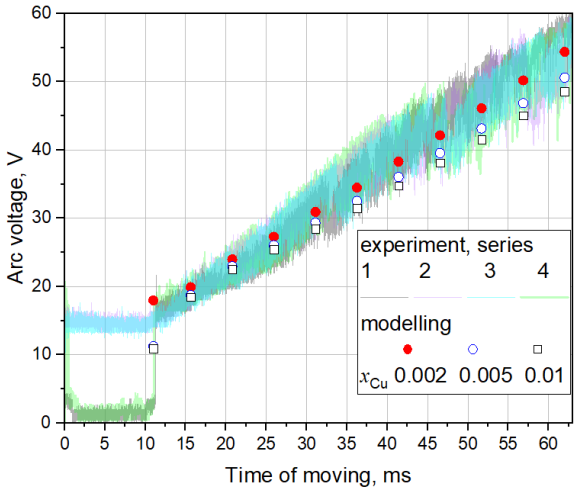

Figure 3. Computed and measured arc voltage during the contact opening. Experimental results of four series are shown and denoted with the numbers 1–4.

FEF=140. Here, the values from four experimental runs are presented. The latter indicate different conditions in the initial phase of the discharge with a fixed gap length of 30 µm. It can be assumed that in some experiments no discharge was initiated. The best agreement of the predicted and measured voltage is obtained for x_{Cu}=0.002. Note that the scattering of the experimental values for a given gap length (to given time of moving) is comparable with the change in the discharge voltage due to variation of x_{Cu}.

Plasma parameters obtained with the factors providing the best matches in Figures 1–3, i.e., F_{Rdis}=1.2, FEF=140, and x_{Cu}=0.002, are shown in Figures 4 and 5. Note that the curves of various colors are used to distinguish the different gap lengths during the contact opening. The spatial distribution of the electric potential (Fig. 4a) indicates a large potential drop in the vicinity of the cathode and the occurrence of multiple reversals of the electric field, while a smaller

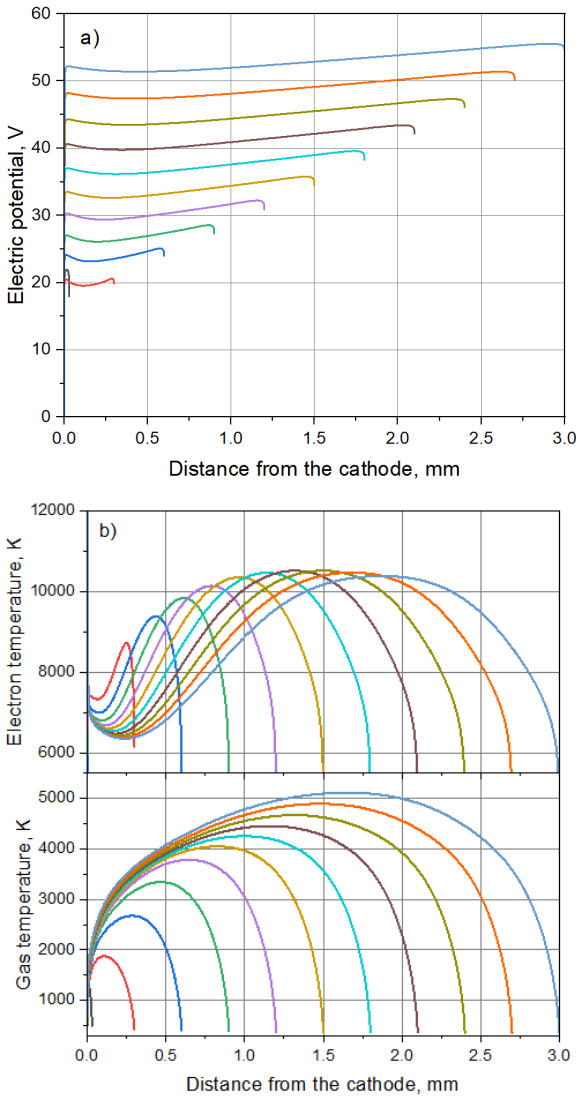

Figure 4. Distributions of a) the electric potential, b) the electron temperature and gas temperature for selected gap lengths during the contact opening. Note that different colors are used to distinguish the results for the selected gap lengths.

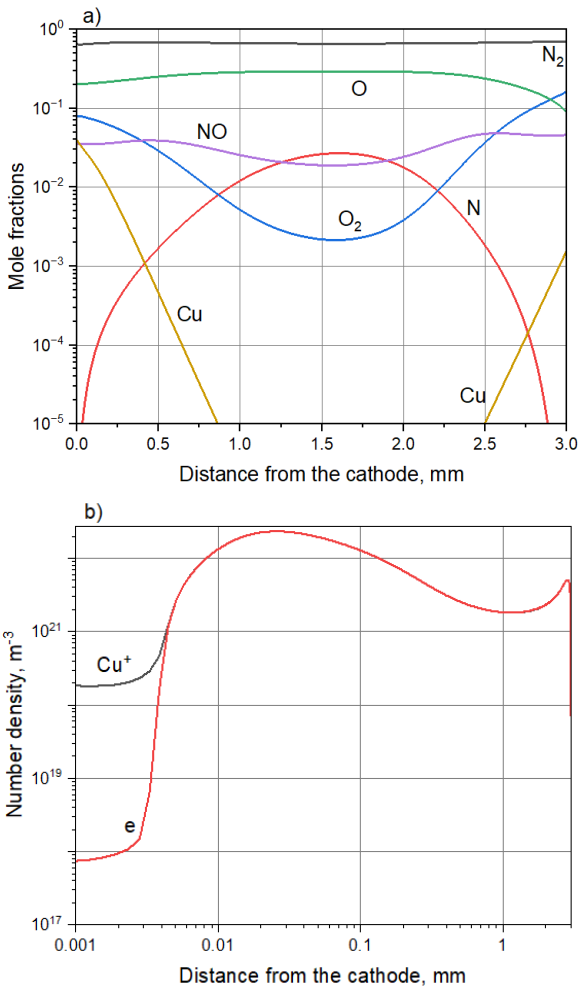

Figure 5. Distributions of the mole fraction of neutral species (a) and number densities of electrons and copper ions (b) for a gap length of 3 mm.

voltage drop is predicted in the vicinity of the anode. A well extended increase of the electric potential from the middle of the gap distance toward the anode can be seen for all selected gap lengths except the initial one (30 µm). This relates to the increase of the electron and gas temperatures (Fig. 4b) in the bulk plasma. Note that the large voltage drop in the cathode space-charge sheath is not resolved in this graph. It should be further noted that the plasma is in thermal non-equilibrium over the all discharge gaps.

Figure 5 shows the distributions of mole fractions of neutral species (a) and number densities of the dominant charged species for a gap length of 3 mm. Note that the dominant neutral species are molecular N_2 and atomic O. The initial average mole fraction of Cu atoms (x_{Cu}=0.002) turns to an increased presence of Cu atoms toward both electrodes. The double log-scale in Figure 5b shows the spatial extent of the cathode space charge sheath ($\sim$ 5 µm) and underlines the dominant role of the Cu^+ ion.

5. Conclusions

This work presents a study of the electrical properties of arcs of length of a few millimeters at a current level of 2 A in atmospheric pressure air. The arcs are burning in the presence of Cu metal vapour. Variations of model parameters (discharge radius, field enhancement factor, mole fraction of Cu atoms) allowed us to achieve a proper match with experimental findings. The behaviour of the plasma parameters is obtained.

6. Data availability statement

The data that support this study are openly available at the following URL/DOI: www.inptdat.de/dataset/Modelling-studies-of-arcs-of-short-length-between-copper-electrodes [12].

Acknowledgements

The work is funded by the German Research Foundation (DFG) Project number 524731006.

References

[1] M. J. Price and F. L. Jones. The electrical contact: the properties and rupture of the microscopic molten metal bridge. *J Phys D: Appl Phys*, 2(4):589, 1969. doi:10.1088/0022-3727/2/4/315.

[2] C. Hollenstein and J.-L. Dorier. Micro-plasma formation during opening of a low current electrical contact. *J Phys D: Appl Phys*, 41(3), 2008. doi:10.1088/0022-3727/41/3/035207.

[3] J. Sekikawa and T. Kubono. Voltage-current characteristics of breaking arc at constant opening speed in the air. *IEEE Trans Compon Packag Technol*, 27(1):167–171, 2004. doi:10.1109/TCAPT.2004.825754.

[4] M. Baeva. Reversal of the electric field and the anode fall in DC arcs in air during contact opening. *J Phys D: Appl Phys*, 57(39):LT01, 2024. doi:10.1088/1361-6463/ad5c73.

[5] M. Baeva and D. Uhrlandt. Modelling of microarcs in copper metal vapour dominated air. *J Phys D: Appl Phys*, 58(9):095204, 2025. doi:10.1088/1361-6463/ad9f79.

[6] R. N. Gupta, J. M. Yos, A. A. Thompson, and G.-P. Lee. *NASA Reference Publication*. 1990.

[7] L. M. Biberman, V. S. Vorob'ev, and I. T. Yakubov. Kinetics of impact-radiation ionization and recombination. *Sov Phys Uspekhi*, 15:375–394, 1973. doi:10.1070/PU1973v015n04ABEH004987.

[8] M. Baeva. Application of the transferred matrix method to a unified evaluation of the cathodic electron emission. *AIP Adv*, 8:085322, 2018. doi:10.1063/1.5041314.

[9] M. J. Zehe, S. Gordon, and B. J. McBride. *NASA TP-2001-210959*. Glenn Research Center, 2001.

[10] A. Gleizes, Y. Cressault, and P. Teulet. Mixing rules for thermal plasma properties in mixtures of argon, air and metallic vapours. *Plasma Sources Sci Technol*, 19:055013, 2010. doi:10.1088/0963-0252/19/5/055013.

[11] J. K. C. Ballentin, M. Baeva, and D. Uhrlandt. Experimental studies of microarcs between copper electrodes in atmospheric pressure air. *Plasma Phys Technol*, 12(2):95, 2025. doi:10.14311/ppt.2025.2.95.

[12] M. Baeva, J. K. C. Ballentin, and D. Uhrlandt. Modelling studies of arcs of short length between copper electrodes - dataset, 2025. doi:10.34711/INPTDAT.942.